Bifurcations from steady sliding to stick slip in boundary lubrication

A. A. Batista and J. M. Carlson
Department of Physics, University of California, Santa Barbara, Santa Barbara, California 93106
(Received 14 August 1997)

We explore the nature of the transitions between stick slip and steady sliding in models for boundary lubrication introduced in J. M. Carlson and A. A. Batista, Phys. Rev. E **53**, 4153 (1996). The models are based on the rate and state approach which has been very successful in characterizing the behavior of dry interfaces [A. Ruina, J. Geophys. Res. **88**, 10 359 (1983)]. Our models capture the key distinguishing features associated with surfaces separated by a few molecular layers of lubricant. Here we find that the transition from steady sliding to stick slip is typically discontinuous and sometimes hysteretic. When hysteresis is observed it is associated with a subcritical Hopf bifurcation. In either case, we observe a sudden and discontinuous onset in the amplitude of oscillations at the bifurcation point. [S1063-651X(98)01605-5]

PACS number(s): 81.40.Pq, 46.10.+z, 46.30.Pa, 83.20.Bg

I. INTRODUCTION

Friction plays a central role in a wide variety of systems. In order to design reliable machines and make accurate predictions for their dynamical response it is necessary to develop models and phenomenological constitutive relations which describe the friction acting between slipping surfaces. Constitutive relations involve mean-field-like dynamical variables which represent the collective evolution of the microscopic degrees of freedom. They play important roles in the design and control of engineering systems such as antilock brakes and nanometer positioning devices [1,2]. Particularly with the development of micromechanical machines, a more complete understanding of friction at molecular scales has become increasingly important [3]. This has led to the development of new experimental tools such as the surface force apparatus (SFA) which allows for the precise measurement of friction in thin lubricant films (see Fig. 1).

In the regime referred to as boundary lubrication atomically flat surfaces are separated by a few molecular layers of lubricant, and the behavior of the interface becomes qualitatively different from the more familiar case of bulk viscosity which is traditionally associated with lubricants. In boundary lubrication the interfacial material can pack into a solidlike structure due to its confinement and exhibit properties such as a finite yield stress and stick slip instabilities (see Fig. 2). [4–6]. Even when the interface slips steadily the frictional resistance can be six orders of magnitude greater than that of the bulk [7]. Certain aspects of this scenario may also be relevant for rough surfaces in which the asperity contacts are separated by thin layers of lubricant, although in that case the friction is likely to involve asperity deformation as well.

Recent experiments have begun to quantitatively capture specific features associated with boundary lubrication at flat interfaces which differentiate the frictional properties of this regime from that of both bulk lubricants and dry interfaces [5,6,8]. The key differences are revealed by studying effects which are time dependent. In contrast to steady state sliding, where the only dynamical variable the friction can depend on is the constant slip speed V, transient effects and stick-slip oscillations reveal the history dependence which to date provides some of the best clues for the microscopic mechanisms which are responsible for the dissipation. Both large scale numerical simulations [9] and more recently experimental studies [10] suggest that sticking of the slider block is associated with a freezing or glasslike transition, while the microscopic signature of the initiation of slip is associated with a shear melting transition in the lubricant layer.

Our study of phenomenological descriptions of boundary lubrication follows a large body of work, primarily within the rock mechanics community, on rate and state laws for dry interfaces which were introduced by Ruina [11]. Ruina's constitutive relation is remarkably effective at capturing steady state and certain transient effects in a wide variety of materials with micron scale roughness [12,13]. The approach involves expressing the friction in terms of the instantaneous slip speed at the interface and one or more state variables, for which phenomenological evolution equations are also introduced. The underlying assumption is that the interfacial area is large enough to be self-averaging, so that a mean-field-like state variable is sufficient to capture the collective dependence of the microscopic degrees of freedom on the dynamical variables—time, displacement, slip speed—that characterize the motion. Of course, this basic approach need not in general apply. Instead it represents an initial attempt to use an underlying physical mechanism to capture observed transient effects which cannot be accounted for in a simple friction law where the force depends only on the instantaneous slip speed.

A great deal of work has been done using Ruina's model. The efforts included parallel experimental study [12,14,23] and in depth dynamical systems analysis [15–18]. The latter has led to important insights into the kinds of transient phenomena which might be expected in systems described by the specific history dependent dynamics described by Ruina's law. This in turn has led to new experimental tests of the applicability of this description.

In terms of the basic phenomenology of friction at interfaces, one of the interesting features of boundary lubrication is that it is clearly different from both dry interfaces and bulk lubrication. We expect there may be interesting relationships between this system and others in which the interface is filled with material (e.g., granular material, foam, or fault

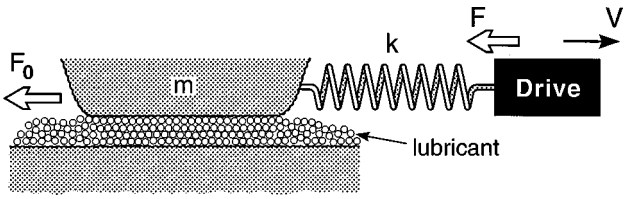

FIG. 1. The SFA experimental setup is mechanically equivalent to a slider block connected to an elastic spring which is pulled at one end at velocity V while in contact with a stationary lubricated surface. The radius of the contact area is of order tens of microns and the thickness of the lubricant is of order 10 Å. Typical drive velocities are in the range 0.001–10 μm/s.

gouge) which may undergo a state change in response to shear. Recently, we proposed a rate and state description for boundary lubrication [19]. As with the experimental system, our model exhibits a discontinuous transition from stick slip to steady sliding which depends on both the drive velocity and the stiffness, illustrated as a function of the drive velocity in Fig. 2. As described in Ref. [19], the model captures additional important features which distinguish boundary lubrication from dry interfaces and which are thought to be associated with the physical mechanism of shear melting and glassy freezing. More recently we have begun to make more detailed quantitative [20] comparisons between our model and the experimental results.

It is the purpose of this paper to explore the properties of these models in the framework of dynamical systems in order to understand its properties in greater depth analytically. In contrast to Ruina's model for dry friction which exhibits a continuous supercritical Hopf bifurcation [13], we obtain a discontinuous transition between stick slip and steady sliding in agreement with the experimental observations. We analyze the transition using linear stability analysis [21], and accompany this with a series of numerical studies which to date yield exclusively discontinuous transitions, in some cases with an absence of hysteresis. In every case we find the transition to stick slip is sudden, with no intermediate regime of small oscillations. Our results give more precise criteria for direct comparisons between phenomenological models, experiments, and atomistic simulations.

In Sec. II we present a brief description of the models we study, as well as some of the experimental and numerical background which has motivated this work. In Sec. III we present our analytical results, explored in greater depth in the Appendix. In Sec. IV we present numerical results for the stable and unstable solutions. We conclude with a discussion in Sec. V.

II. BACKGROUND: EXPERIMENTS, NUMERICS, AND PHENOMENOLOGY

The experiments of Israelachvili and his co-workers have yielded many new insights into the nature of friction and lubrication [4–6]. Their results have been obtained using a surface force apparatus (SFA), which consists of two atomically smooth mica cylinders, separated by a few molecular layers of lubricant, and sheared at right angles via an adjustable coupling spring. Elastic deformation due to the normal load flattens the contact surfaces, so that the interface is accurately represented by the schematic diagram in Fig. 1. The upper cylinder corresponds to the rigid slider block which rests on a stationary surface, represented by the lower cylinder. The block is connected to a spring of strength k, which corresponds to the linear elastic response of the SFA driver, and the other end of the spring is pulled forward at velocity V. Because the interface is smooth, flat, and rigid (at least when compared with the lubricant), one can be reasonably confident that variations in the frictional resistance are associated with dynamically induced variations in the lubricant. Note, however, that interactions between the mica and the lubricant due to different relative crystallographic orientations of the upper and lower plates can play an important role, as can additional parameters such as the load, the temperature, the number of layers of the lubricant, and its chemical composition. For the purpose of this paper we will assume these parameters are fixed, and instead focus our attention on the behavior of the system as a function of the external mechanical variables which are most directly associated with the driver, that is the elastic coupling k and pulling speed V.

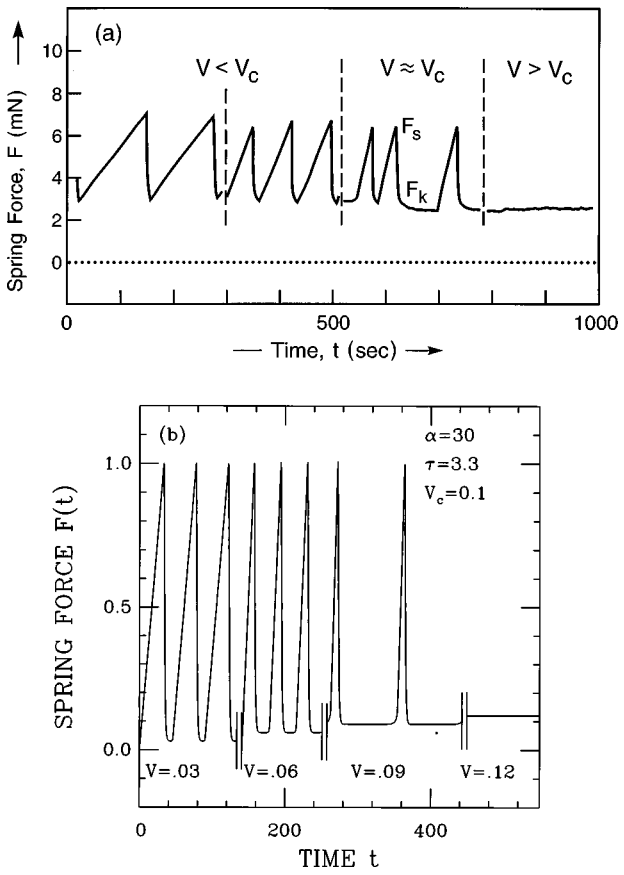

FIG. 2. Traces of the spring force F as a function of time for increasing pulling velocities V. (a) illustrates experimental data from [6] for a hexadecane film at 17 °C ($T<T_c$) with step increases in velocity V marked by the dotted lines. The critical velocity for this system is $V_c \approx 0.4\ \mu$/s. (b) illustrates numerical solutions for model I with the parameter values marked in the figure. The results are presented in terms of the dimensionless units. In each case there is a discontinuous transition from stick-slip behavior to steady sliding at $V=V_c$, which we take to be the first velocity at which the stick-slip spikes disappear as the velocity is increased in small steps.

The equation of motion for the slider block is given by

$$M\ddot{U} = -k(U - Vt) - F_0(\theta, \dot{U}), \tag{1}$$

where $U(t)$ is the displacement of the upper block, and dots denote derivatives with respect to time t. The goal of these experiments is to determine the interfacial friction F_0 by monitoring the spring force $-k(U-Vt)$ as a function of time. In principle F_0 depends not only on the instantaneous slip speed, but also on the slip history and the microscopic configuration of the lubricant.

In a Newtonian fluid the resistance is simply proportional to the slip speed and captured by a single parameter, the friction coefficient β, so that $F_0 = \beta\dot{U}$. When this friction law is substituted into Eq. (1) all initial conditions converge to the steady sliding state $\dot{U}(t) = V$ for any value of k and V.

The surprising new results obtained by Israelachvili and his co-workers were the observations that as the thickness of various lubricants was reduced to molecular dimensions, the fluidlike properties of the interface were replaced by features more reminiscent of solids [4]. In particular, they observed that the films could support a finite shear stress and exhibit either stick slip dynamics or steady sliding depending on a variety of experimental parameters including k and V. Using molecular dynamics (MD) simulations Thompson and Robbins studied boundary lubrication in the underdamped regime [9,22]. Based on their results they suggested that the onset of slipping on each stickslip cycle coincides with shear melting of the lubricant layer, and that the transition to steady sliding could be identified with conditions under which the energy supplied to the system during slip was just large enough to prevent the system from refreezing.

Phenomenologically, it is possible to obtain stickslip solutions to Eq. (1) using a wide variety of friction laws. For example, if we restrict our attention to the subset of friction laws which depend only on the instantaneous velocity $F_0(\dot{U})$, steady sliding states are unstable over any range of velocities where F_0 exhibits velocity weakening. Furthermore, a transition to steady sliding could be associated with a crossover to a velocity-strengthening regime in F_0. However, this approach predicts that the transition depends only on the drive velocity V, which violates experimental observations in which the transition to steady sliding may also be associated with an increase in stiffness.

A more accurate description of the data can be obtained by including history-dependent effects in the friction law. In the case of dry friction at rough interfaces, Ruina introduced a rate and state constitutive relation which captures certain experimental aspects (the transients associated with velocity shifts in the steady sliding regime) of that system surprisingly well [11–13,23,24]. More recently, Caroli *et al.* [25] modified the model to give a better fit to the dynamical phase diagram as a function of k and V for that system.

The rate and state approach is a phenomenological fit to the data, in which the friction is written as a function of the instantaneous slip speed $\dot{U}$ and one or more state variables θ_i: $F_0(\dot{U}, \{\theta_i\})$. The primary justification for including multiple state variables arises when multiple time and/or length scales are relevant in the problem. The state variables are described by evolution equations $\dot{\theta}_i = \Theta_i(\dot{U}, \{\theta_i\})$, so that when combined with the equation of motion, the system is described by two or more coupled ordinary differential equations (ODE's). This approach assumes that microscopic fluctuations in the state of the lubricant can be neglected in the equations of motion, on the basis that their time scales are very small compared to those characteristic of the macroscopic degrees of freedom of the system as a whole, and occur on length scales which are small compared to the contact area.

Previously we proposed a rate and state law for the case of boundary lubrication [19]. We defined the friction to be a continuous function, depending on the rate and a single state variable, with the simplest possible dependence (linear) on these arguments:

$$F_0 = \begin{cases} (-\infty, \sigma\theta], & \dot{U} = 0 \\ \sigma\theta + \beta\dot{U}, & \dot{U} > 0. \end{cases} \tag{2}$$

We loosely associate θ with the degree to which the lubricant is melted. The evolution equations (below) will be defined so that θ is positive and bounded above and below. Large values of θ correspond to a more solidlike lubricant with higher frictional resistance, while lower values of θ correspond to a more melted lubricant, with a smaller state-dependent contribution to the resistance. We express the two contributions to the sliding friction ($\dot{U} > 0$) in terms of a standard Newtonian term $\beta\dot{U}$ and the state term $\sigma\theta$. Here σ represents the load, so that the friction is proportional to load in the more solidlike elastic regime.

The two models we will consider differ (in a fairly minor way) in terms of the evolution equations for the state variable. We refer to the original model as model I and the new model as model II. We introduce two models primarily for technical reasons, which will become apparent as we proceed with our analysis. However, it will be interesting to note how small changes in the phenomenological equations can result in changes in the nature of the bifurcation.

The evolution equation for model I is given by

$$\dot{\theta} = (\theta - \theta_m)\left[\frac{(\theta_M - \theta)}{\tau} - \alpha\dot{U}\right]. \tag{3}$$

The evolution equation for model II is given by

$$\dot{\theta} = (\theta - \theta_m)\left[\frac{(\theta_M - \theta)}{\tau} - \alpha(\theta - \theta_m)\dot{U}\right]. \tag{4}$$

The two models thus differ only by the extra factor of $(\theta - \theta_m)$ in the last term.

Both of these equations are motivated by Thompson and Robbins' numerical evidence that the lubricant layer melts in response to shear. Here the state variable is loosely associated with the degree to which the lubricant layer is melted. The minimum value $\theta = \theta_m$ correspond to a fully melted layer, and the maximum value $\theta = \theta_M$ corresponds to the fully frozen case. Equations (3) and (4) are constructed so that any initial state $\theta_m < \theta < \theta_M$ remains bounded in this interval.

The first term on the right-hand side of both of the evolution equations is the simplest way to describe the fact that in the absence of shear stress (zero shear velocity $\dot{U} = 0$) the

melted phase is unstable and the frozen state is stable. From any initial state $\theta_0 \neq \theta_m$ the film approaches the frozen state at a rate which is proportional to τ with a sharp increase at a characteristic time t^* (derived in [19])

$$t^* = \frac{\tau}{(\theta_M - \theta_m)} \ln\left(\frac{\theta_M - \theta_0}{\theta_0 - \theta_m}\right) \approx -\frac{\tau \ln(\theta_0 - \theta_m)}{\theta_M - \theta_m}. \quad (5)$$

The closer the initial state is to the fully melted configuration the longer it takes for the system to freeze. For the slider block described by Eq. (1) the monotonic increase of θ corresponds to a steady increase in the static friction, which approaches some asymptotic limit as $t \to \infty$ in agreement with experimental observations.

The second terms on the right-hand sides of Eqs. (3) and (4) describes the tendency of the film to become increasingly melted as the block begins to slip. Assuming the block is initially at rest at the origin and is subject to a constant pulling speed V (for convenience here assumed to be small) the onset of slip occurs at time $t_0 = \theta_M / kV$, where we assume the value of θ at the onset of slip is $\theta \approx \theta_M$. If the healing time τ is large, then the first term on the right can initially be ignored. For model I we obtain an exponential decay of the friction with accumulated slip $(\theta - \theta_m) \approx (\theta_M - \theta_m)\exp^{-U/\alpha}$, while for model II we obtain power-law relaxation $(\theta - \theta_m) \approx [\alpha U + 1/(\theta_M - \theta_m)]^{-1}$. In both cases, melting occurs over a characteristic length $1/\alpha$.

Most of the parameters in these models can be estimated based on observations. The minimum value of the state variable θ_m is approximately equal to zero, so that the friction is taken to be purely viscous in this regime [26]. The maximum value θ_M is set by the maximum static friction, obtained in terms of the peak spring force prior to slip following long intervals in which the block is at rest. Experimentally, the characteristic freezing time τ has been estimated using a specific time-dependent driving referred to as a ''stop-start'' experiment. Here the slider block is pulled at velocity V in the steady sliding regime, then the pulling is ceased altogether for a time interval τ_S, after which it is recommenced at the initial speed V. The spring force is measured, and for stopping times less than a characteristic nucleation time τ_N the mass begins sliding as soon as pulling is reinitiated and the spring force returns smoothly to its original value. On the other hand, if $\tau_S > \tau_N$ the block remains stuck until the applied stress exceeds the yield stress at which point the block begins to slide. This is manifest in an observed peak, or stiction spike, in the spring force, which has a sharp onset at $\tau_S \approx \tau_N$. Models I and II exhibit this behavior as well, and the stop time associated with the experimental emergence of the stiction spike can be mapped onto the model value t^* [Eq. (5)] giving a fit to the variable τ. We also expect that τ will be sensitive to temperature T, increasing with increasing temperature, and approaching infinity at the melting temperature $T = T_m^c$ of the film. With current experimental information, the most difficult parameter to estimate is the characteristic melting length $1/\alpha$. We expect α to be a monotonically increasing function of the film thickness, so that we obtain only bulk viscosity when the lubricant film is very thick. For now we will leave α as an almost free parameter for fitting our results with data from MD computer simulations or experiments.

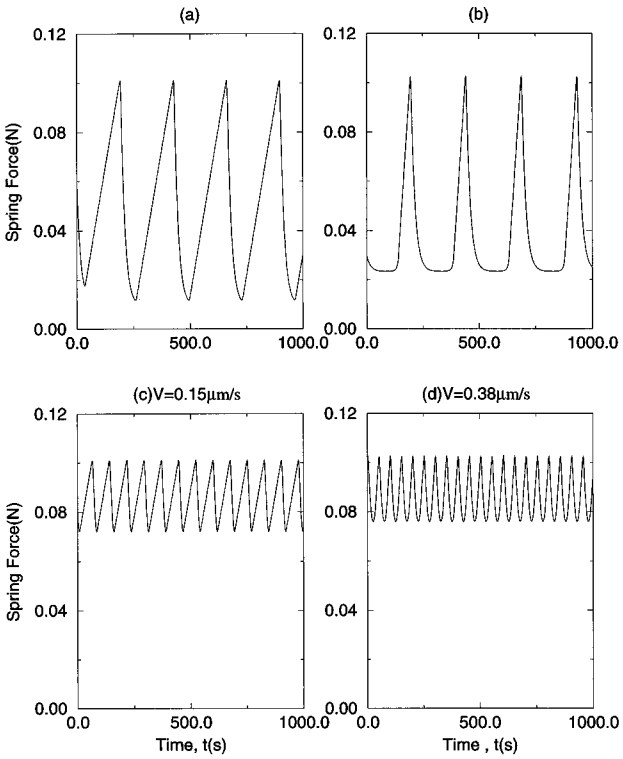

FIG. 3. Traces of the spring force $-k(U - Vt)$ as a function of time for increasing pulling velocities V, obtained as numerical solutions to Eqs. (8) in (a) and (b) and Eqs. (19) in (c) and (d). In each case we set the parameters according to experimental estimates: $\tau = 2$ s, $\sigma = 100$ mN, $\theta_m = 0$, $\theta_M = 1$, $\beta = 6 \times 10^4$ Pa s m, and $1/\alpha = 1$ μm (see text), and take $k = 3.5$ kN/m. For both models we observe a discontinuous transition from stick slip to steady sliding at a value $V = V_c$, defined to be the first velocity at which the stick-slip spikes disappear (and the spring force becomes constant with time) as the velocity is increased in small steps. At this value of k for model I $V_c = 0.475$ μm/s, and for model II $V_c = 0.397$ μm/s.

III. ANALYTICAL RESULTS

In this section we present a bifurcation analysis of Eqs. (1)–(4). We focus our attention on the behavior of the models as a function of the stiffness k and drive velocity V. We assume the system is in the overdamped limit, in agreement with our best fits to experimental data [19,20]. This allows us to drop the inertial term in Eq. (1).

For large values of k and V both models exhibit only steady sliding solutions, characterized by constant spring force. However, when k and V are decreased sufficiently there is a transition to stick slip solutions such as those in Fig. 3, where we illustrate a series of stick-slip pulses obtained numerically for models I [(a) and (b)] and II [(c) and (d)]. The results are obtained using the same parameter values at fixed k with two different (increasing in this case) drive velocities. In spite of the similarity of the models, the slip pulse shapes are quite different, with model I exhibiting extended periods of almost steady sliding as the transition is approached. While the slip pulses obtained for model I are of comparatively greater duration and period, at these parameter settings model I is further from the transition velocity than model II.

We begin our analysis with model I, followed by a summary of the relevant differences obtained for model II. We

first rewrite the equations in terms of dimensionless variables:

$$\tilde{t}=\frac{k}{\beta}\,t,$$

$$\tilde{\tau}=\frac{k\tau}{\beta\theta_M},$$

$$\tilde{U}=\frac{k}{\sigma\theta_M}\,U,$$

$$\tilde{\alpha}=\frac{\sigma\theta_M}{k}\,\alpha,$$

$$\tilde{V}=\frac{\beta V}{\sigma\theta_M},$$

$$\tilde{\theta}=\theta/\theta_M. \tag{6}$$

Times have been scaled by the characteristic time β/k associated with the exponential relaxation of a simple overdamped oscillator (with no state variable) to the steady sliding state. Our scaling of the freezing time τ includes a (dimensionless) factor of θ_M which accounts for the magnitude of the state variable in the asymptotic frozen state. Displacements have been rescaled by the characteristic slip displacement $\sigma\theta_M/k$ of an undamped oscillator which begins to slip when the spring force reaches the maximum static friction and resticks when the slip speed returns to zero. The state variable is scaled by its maximum value, so that in rescaled units $0<\tilde{\theta}<1$.

It is most convenient to analyze the coupled ODE's [Eqs. (1)–(3)] as an autonomous system, so we also transform to a reference frame moving at the drive velocity

$$\tilde{U}'=\tilde{U}-\tilde{V}\tilde{t}. \tag{7}$$

Finally dropping the tildes and primes, when the block is sliding our system becomes

$$\dot{U}=-U-\theta-V,$$

$$\dot{\theta}=\theta\left[\frac{(1-\theta)}{\tau}+\alpha(U+\theta)\right]. \tag{8}$$

Equations (8) always exhibit a steady state solution of the form

$$U_{\rm ss}^{\rm I}=-(\theta_{\rm ss}^{\rm I}+V) \tag{9}$$

and

$$\theta_{\rm ss}^{\rm I}=\begin{cases}1-\alpha\tau V, & V<1/\alpha\tau\\ 0, & V>1/\alpha\tau,\end{cases} \tag{10}$$

which is obtained from Eqs. (8) by setting $\dot{U}=\dot{\theta}=0$. In the original reference frame this solution corresponds to the block slipping uniformly at the pulling speed. One awkward feature of model I is the fact that the steady state value of θ is zero for pulling speeds greater than $1/\alpha\tau$. While $\theta=0$ can only be obtained in asymptotic time from Eqs. (8), θ does become very small quickly, slowing the evolution dramatically. This can lead to pathological effects at high speeds. For example, the freezing time as measured in stop-start experiments becomes unrealistically dependent on the cumulative slipping time preceding the stopping interval. In our previous studies we have avoided this high speed regime. This feature does not arise at all in model II. In that case, the steady state value of θ decreases smoothly towards zero as $V\to\infty$ in contrast to the piecewise linear form given in Eq. (10).

A straightforward linear stability analysis of this solution yields the bifurcation point, where the steady sliding solution becomes unstable to stick slip. To this end, we again change variables, this time so we can linearize about steady sliding state:

$$U=U_{\rm ss}^{\rm I}+x,$$

$$\theta=\theta_{\rm ss}^{\rm I}+y. \tag{11}$$

Retaining only the linear terms in x and y we obtain

$$\begin{pmatrix}\dot{x}\\ \dot{y}\end{pmatrix}=J^{\rm I}\begin{pmatrix}x\\ y\end{pmatrix}. \tag{12}$$

Here the Jacobian matrix is given by

$$J^{\rm I}=\begin{pmatrix}-1 & -1\\ \theta_{\rm ss}^{\rm I}\alpha & \theta_{\rm ss}^{\rm I}(\alpha-1/\tau)\end{pmatrix}. \tag{13}$$

The equation for the eigenvalues of J^I is

$$\lambda^2-\lambda\,{\rm Tr}J+{\rm det}J=0 \tag{14}$$

from which we see that the eigenvalues are complex conjugates with real part $\gamma={\rm Tr}J/2$ and imaginary part $\Omega=\pm\sqrt{{\rm det}J-({\rm Tr}J/2)^2}$. In the steady sliding regime $V>V_H^{\rm I}$ the real parts are negative ($\gamma<0$). At the bifurcation point $V=V_H^{\rm I}$ they cross the imaginary axis ($\gamma=0$). And in the stick-slip regime they are positive ($\gamma>0$). For this specific model we find

$$\gamma=-\alpha(\alpha\tau-1)(V-V_H^{\rm I}),$$

$$\Omega=\sqrt{1/(\alpha\tau-1)-\gamma^2}. \tag{15}$$

We also have at the bifurcation point $\Omega\neq0$ and $d\gamma/dV\neq0$. These are the necessary requirements for a Hopf bifurcation, and it occurs at the pulling speed

$$V_H^{\rm I}=\frac{1}{(\alpha\tau)}\left[1-\frac{1}{(\alpha-1/\tau)}\right]. \tag{16}$$

In other words, if we begin in the steady sliding state, and decrease the velocity with all other parameters remaining fixed, the constant velocity solution becomes unstable to small perturbations when $V=V_H^{\rm I}$. Reintroducing dimensional variables, we find $V_H^{\rm I}$ decreases linearly with increasing stiffness k:

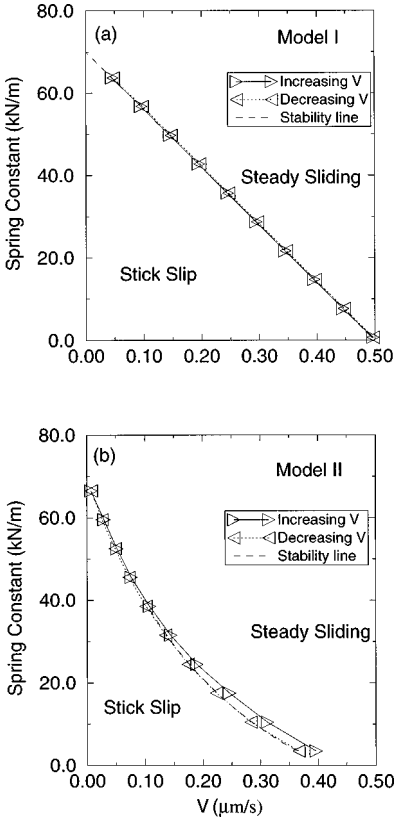

FIG. 4. Dynamical phase diagram for (a) model I, with parameters set by experimental values (see text). Numerical simulations for the phase boundary agree with the linear stability analysis presented in Sec. III. The transition is observed to be discontinuous, but not hysteretic. (b) represents the analogous results for model II. Here the transition is hysteretic, in agreement with the normal forms bifurcation analysis.

$$V_H^{\mathrm{I}}=\frac{\theta_M^2}{(\alpha\tau)}\left[1-\frac{k}{(\sigma\alpha-\beta/\tau)\theta_M}\right]. \tag{17}$$

From Eq. (17) we see there is a maximum stiffness $k_{\max}$ at which $V_H^{\mathrm{I}}=0$. For $k>k_{\max}$ the steady state solution remains stable for all pulling speeds V.

These results are summarized in the dynamical phase diagram illustrated in Fig. 4, in which we have set our parameters according to estimated experimental values [6,10]. In particular, we take $\tau\approx 2$ s on the basis of fits to the stop-start experiments. Typical loads are of order $\sigma=100$ mN, and $\theta_M\approx 1$ based on peak values of the static friction. The friction coefficient is estimated to be $\beta\approx 6\times 10^4$ Pa s m [27]. The free parameter α is set using the transition velocity $V_H\approx 10$ μm/s for a specific value of $k=440$ N/m. This yields $1/\alpha\approx 1$ μm. The rest of Fig. 4 is generated using these values in Eq. (17) as the stiffness ranges between its maximum $k_{\max}=7\times 10^4$ N/m and minimum values $k_{\min}=0$.

The natural next step in analyzing the bifurcation would be to determine via normal forms whether the bifurcation is predicted to be subcritical or supercritical. For model I, the leading term in this analysis is zero (see the Appendix) which is inconclusive, albeit consistent with our numerical observation of a discontinuous, nonhysteretic transition from steady sliding to stick slip. It is primarily for this technical reason that we introduced the alternative model II. We have no strong *a priori* basis to prefer one model over the other at this point. Technically model I involves slightly simpler functional forms, while model II avoids pathological behavior in the high velocity regime. In principle, we expect the best fit of the data would be obtained in terms of a systematic (e.g., polynomial) expansion of the friction and evolution equations in Eqs. (2) and (3). Of course that would involve a tradeoff between the number of parameters and the complexity of the model versus accuracy of the data fit.

Now we outline the modifications to the above calculations which we obtain for model II. The transformation which leads to dimensionless variables is the same as that given in Eq. (6) for model I with the exception of the rescaling of α, which now is given by

$$\tilde{\alpha}=\frac{\sigma\theta_M^2\alpha}{k}. \tag{18}$$

This leads to rescaled equations in the moving frame [analogous to Eqs. (8)] which are of the form

$$\dot{U}=-U-\theta-V,$$

$$\dot{\theta}=\theta\left[\frac{(1-\theta)}{\tau}+\alpha(U+\theta)\theta\right]. \tag{19}$$

The steady sliding solution, analogous to Eqs. (9) and (10), is given by

$$U_{\mathrm{ss}}^{\mathrm{II}}=-\theta_{\mathrm{ss}}^{\mathrm{II}}-V \tag{20}$$

and

$$\theta_{\mathrm{ss}}^{\mathrm{II}}=\frac{1}{1+\alpha\tau V}. \tag{21}$$

As previously mentioned, $\theta_{\mathrm{ss}}^{\mathrm{II}}$ is smooth and positive here, rather than being piecewise linear and zero for larger pulling speeds.

As before [Eqs. (11)] we linearize about the steady sliding solution to determine the Hopf bifurcation point. The Jacobian matrix analogous to Eq. (13) is

$$J^{\mathrm{II}}=\begin{pmatrix}-1 & -1\\ (\theta_{\mathrm{ss}}^{\mathrm{II}})^2\alpha & \alpha(\theta_{\mathrm{ss}}^{\mathrm{II}})^2-1/\tau\end{pmatrix}. \tag{22}$$

The real and imaginary parts of the eigenvalues of J^{II} near the bifurcation point are

$$\gamma=-\alpha^2\tau\theta_{\mathrm{ss}}^3(V-V_H^{\mathrm{II}}),$$

$$\Omega=\sqrt{1/\tau-\gamma^2}, \tag{23}$$

which obey the requirements for the Hopf bifurcation. Again we locate the transition by determining when the real part of the eigenvalues of J^{II} cross the imaginary axis: $\mathrm{Tr}J^{\mathrm{II}}=0$. This yields

$$V_H^{\mathrm{II}}=\frac{1}{\alpha\tau}\left[\sqrt{\alpha\tau/(\tau+1)}-1\right]. \tag{24}$$

Reintroducing the dimensional variables we obtain V_H again as monotonically decreasing function of k, but no longer linear:

$$V_H^{\mathrm{II}}=\frac{\theta_M}{\alpha\tau}\left[\sqrt{\frac{\alpha\tau\sigma\theta_M}{k\tau+\beta}}-1\right]. \tag{25}$$

Results for realistic experimental parameters are illustrated in Fig. 4. Here we have taken the same parameters as used in model I, and again find $\alpha^{-1}\approx 1\ \mu$m by fitting Eq. (25) to the particular data point $V_H=10\ \mu$m/s and $k=440$ N/m. From Eq. (25) we obtain the same value of $k_{\max}$, the maximum stiffness associated with stick slip, as obtained for model I. The phase boundary curves in this case yielding a somewhat better fit to experiments, which exhibit a power-law dependence of V_H on k over the range of k considered [10].

One of the main advantages in studying model II is the fact that the normal forms analysis does produce a nonzero value for the stability coefficient a_1 which predicts the nature of the transition (see the Appendix). The basic method is outlined in [28], and involves another change of variables to radial and angular coordinates associated with the amplitude of the oscillating solution and its phase. At the Hopf bifurcation point, the amplitude becomes nonzero. Supercritical bifurcations are associated with continuous growth of the amplitude of oscillations and are predicted by a negative stability coefficient a_1, while subcritical bifurcations are associated with discontinuous changes and are predicted by a positive stability coefficient a_1. For model II we obtain

$$a_1^{\mathrm{II}}=\frac{\alpha}{8}\left(\frac{3}{\tau}-1\right) \tag{26}$$

which allows for the possibility of either a direct or an indirect transition, depending on the values of the parameters. Our estimates of realistic parameter values correspond to the subcritical case. This is consistent with most experiments to date which typically exhibit discontinuous transitions with intermittent stick slip observed in the neighborhood of $V_c(k)$.

IV. NUMERICAL RESULTS

In this section we present a summary of our numerical results for the dynamical phase diagrams of model I and model II (Fig. 4). We have both confirmed the results of our stability analysis in Sec. III for the transition from steady sliding to stick slip, and checked for hysteresis by traversing the transition in the opposite direction. In each case we have set our parameters to realistic values, as discussed in Sec. II.

We obtained our results by integrating Eqs. (8) and (19) incorporating the static friction condition given in Eq. (2) when appropriate. We used a fourth-order Runge-Kutta algorithm [29] with a fixed step size $h=5\times10^{-5}$. This choice of h is much less than any relevant time scale for the dynamics: for model I the period of small oscillations at the bifurcation point is approximately 9.6 in our dimensionless units, while for model II the period is at least 0.96.

The dynamical phase diagrams as a function of k and V are illustrated in Fig. 4. Each point on the boundary between stick slip and steady sliding is obtained by increasing V in small steps $\Delta V=0.001$ and then integrating for $\Delta t=400$ in order for the system to reach a new periodic steady state before the pulling speed is again increased. Some representative stick slip solutions are illustrated in Fig. 3. In this direction the transition is identified with the first value of V for which the block fails to restick. At this value of V and beyond in both models we find that the new stable solution corresponds to the constant velocity steady sliding state, with no intermediate regime of small oscillations.

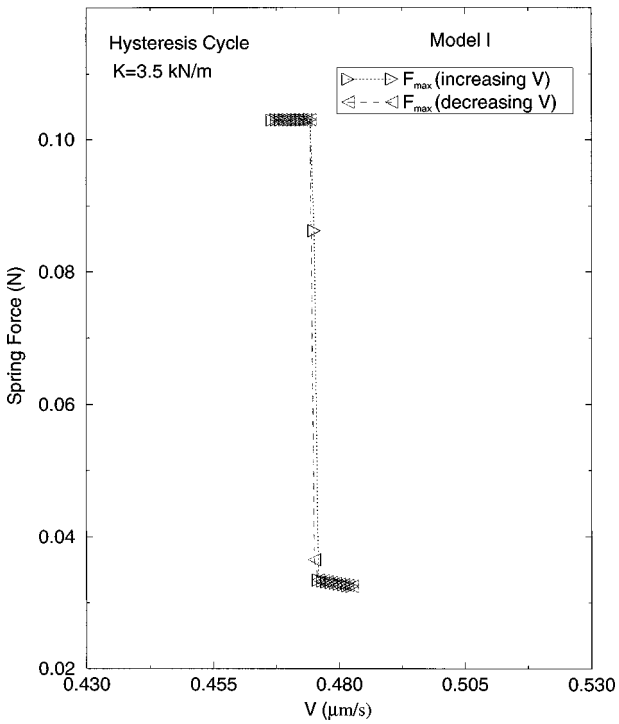

FIG. 5. Sample bifurcation diagram for model I. We plot the maximum spring force as a function of V for fixed $k=3.5$ kN/m. The small hysteresis observed here is a transient associated with the finite integration time at each value of V, and decreases as the integration time is increased.

To locate the boundary traversing the transition in the opposite direction (from the steady sliding side), we ramp down the pulling speed in small steps $\Delta V=-0.001$ for each fixed value of k. In this case, small perturbations are applied to the steady sliding solution, and the transition is associated with the value of V at which the perturbations first begin to grow. For these models, we have always found that the stable solution eventually converges to periodic stick slip oscillations.

The results presented in Fig. 4 illustrate that for model I there is no hysteresis: the phase boundary computed numerically in both directions agrees well with the results of our stability calculations in Sec. III. Note that for any finite integration time Δt, the numerical solution will suggest a nonzero hysteresis loop as shown in Fig. 5, where we plot the maximum spring force of the stable solution as a function of pulling speed V for fixed k. The transition is associated with the sharp drop from (essentially) the value associated with the static friction maximum in the stick slip phase, to the steady state value $F_0(V)$ which corresponds to steady sliding. Apparent hysteresis occurs in this numerical calculation because just above the transition (approached from the

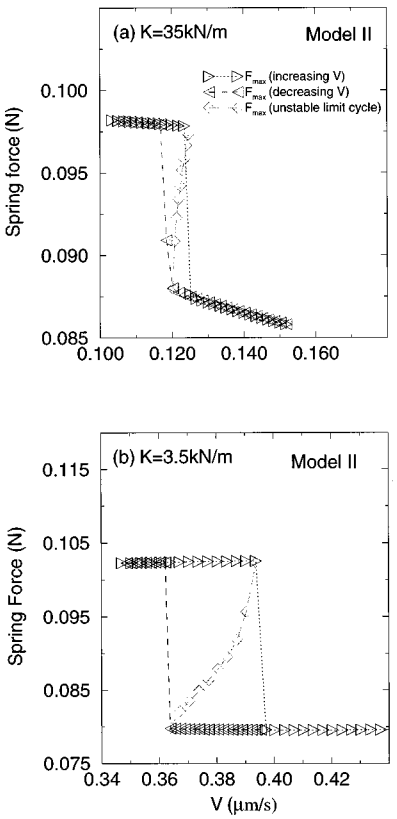

FIG. 6. Sample bifurcation diagrams for model II for (a) $k=35$ kN/m and (b) $k=3.5$ kN/m. The width of the hysteresis cycle decreases with increasing k as predicted by the normal forms calculation.

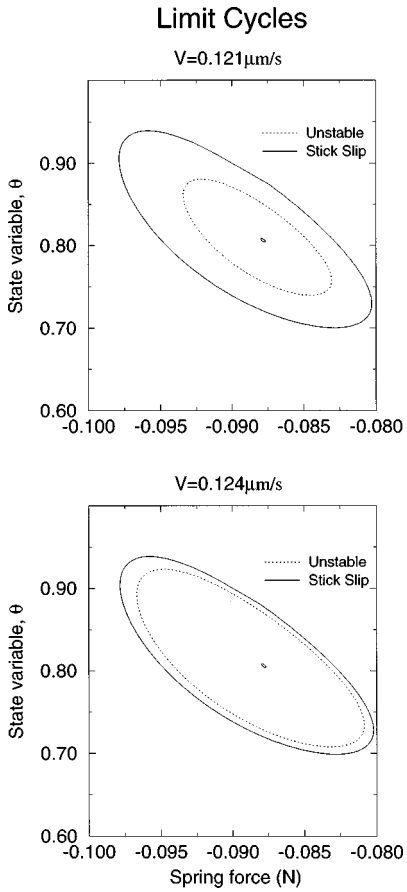

FIG. 7. A phase portrait of the unstable limit cycles and the stick-slip limit cycles. Note that as we increase V from the transition point V_H^{II} the unstable cycle grows until it collides and eliminates the stick-slip cycle, as illustrated in terms of the maximum spring force in Fig. 5. Results are shown for $k=35$ kN/m. The small dot in the middle of the limit cycles marks the stationary point.

stick slip side) the rate at which the solution converges to steady sliding is very small. While the real part of the eigenvalue of the Jacobian (13) is negative in the steady sliding phase, it crosses zero at the transition point. Thus, as we approach the transition from either side the growth (decay) rate of small perturbations approaches zero. By increasing the integration time Δt we have confirmed that the size of the hysteresis loop for model I decreases appropriately, so that in the limit $\Delta t \to \infty$ we expect the phase boundaries to coincide exactly.

In contrast, for model II we clearly obtain hysteretic transitions which are not sensitive to the integration time Δt. Our numerical results for the transition from steady sliding to stick slip do coincide with the stability analysis as expected, but the transition associated with increasing V occurs at a higher value than that which we observe on the way down. Sample hysteresis loops are illustrated in Fig. 6 where we plot the maximum spring force as a function of pulling speed V for two different values of the stiffness k. Figure 6(a) illustrates our results for a comparatively large value of k, where the width of the hysteresis loop is observed to be relatively small compared to smaller values of k, as illustrated in 6(b). This is consistent with our normal forms bifurcation analysis presented in the Appendix, where we find that the rate of growth of the unstable limit cycle increases with increasing k, suggesting a more rapid approach to the stable stick slip cycle in the case of large k.

To determine the amplitudes of the unstable limit cycles which are included in Fig. 6, we used the Poincaré map. We begin with a small perturbation to the stationary point and allow the solution to flow for one loop in the phase space, defined by the state variable and spring force $[\theta, -k(U-Vt)]$ (see Fig. 7). The amplitude of the initial perturbation is subsequently increased along a fixed axis from the stationary point towards the stick slip orbit until we find the unstable limit cycle. The only closed orbits in the phase space are the stationary point, the stable stick slip solution, and the unstable orbit (which oscillates without coming to a complete stop). Initial conditions which flow towards the stationary point flow lie within the unstable limit cycle, while initial conditions which flow towards the periodic stick slip solution are outside the unstable orbit. Some sample stable and unstable orbits are illustrated in Fig. 7.

V. CONCLUSIONS

We have studied dynamical phase transitions in two models of boundary lubrication. In both cases, our numerical simulations have shown that the transition is strongly discontinuous, exhibiting a crossover from uniform steady sliding directly to large amplitude stickslip oscillations. Linear stability analysis of these models [Eqs. (17) and (25)] yields excellent agreement with our numerical results as the velocity is lowered or spring constant is decreased.

Discontinuous transitions to oscillatory states are typically described by subcritical Hopf bifurcations. Indeed, our results for the stability coefficient for model II show that for realistic parameter values this is indeed the case. Subcritical Hopf bifurcations are accompanied by hysteresis, so that upon raising the velocity or increasing the stiffness, the steady sliding is resumed beyond the point where it was observed when the transition was traversed in the opposite direction. We observe this numerically in model II.

The behavior we observe originally in model I is more unusual. That is, the transition is discontinuous, but not hysteretic. This is consistent with, but certainly not proved by our result that to leading order the stability coefficient is zero in that case. A stronger confirmation is obtained comparing the stability calculation with our previous results in which we calculated an approximate stick slip solution $U(t)$ which was no longer self-consistent along the phase boundary $V_c(k)$ [19]. In the regime in which the approximations were valid, that result agrees with the result obtained here.

The primary goal of these studies is to develop a better understanding of experimental systems, and the kinds of rate and state friction laws that might describe them. For boundary lubrication, a great deal remains to be done in this regard. Phenomenological models such as those we have considered are based on physical insight and represent reasonable guesses for frictional constitutive relations. The underlying mechanism that the model assumes is based on molecular scale simulations, and the basic qualitative properties of the models agree with observations. One of the most important messages we extract from the phenomenological approach is that history dependence is of fundamental importance, and needs to be the focus of experimental measurements as well as microscopic models and simulations.

Our calculations open up the possibility for more detailed quantitative comparisons between experiments and these two specific phenomenological models. However, we are not yet at a point where we can expect perfect agreement. When phenomenological constitutive relations fit the data well, they can be important technologically. However, this typically would require a systematic expansion involving large numbers of parameters, and the data is not sufficiently precise at this point to warrant such an approach. Still it is important to think about these comparisons as stepping stones to finding better models and planning experiments which will guide their development.

Indeed, a detailed comparison of model I and experiments is presented in [20]. Most of the experimental results for dynamical phase diagrams which have been obtained to date are somewhat more analogous to the results we have obtained here for model II, though even in that case the fit is far from perfect [10]. For lubricants such as tetradecane the relationship between the transition velocity V_c and the stiffness k is reasonably well described by a power law [$V_c(k) \sim 1/k^{\gamma}$ with $1<\gamma<3$], as opposed to the linear relation in Eq. (17). Experimentally the final crossover is marked by a range of velocities over which intermittent stick slip is observed, which can make it difficult to sharply define a transition point. Some lubricants such as OMCTS have exhibited continuous as well as discontinuous transitions. Experiments to determine the dynamical phase diagram as a function of V and k as well as external parameters such as temperature, hydration, and load for cases which exhibit this range of behaviors would be of particular interest.

ACKNOWLEDGMENTS

This work was supported by a grant from the David and Lucile Packard Foundation and NSF Grant No. DMR-9510394. A. A. Batista also thanks the Brazilian Agency CAPES for its ongoing financial support.

APPENDIX: BIFURCATION ANALYSIS

In this Appendix we present a more complete description of the steps which led to our results for the stability coefficients for model II in Sec. III. The null result obtained to leading order for model I can be obtained using the same method, which is outlined in detail in Ref. [28].

The full nonlinear ODE system in the variables x and y which are centered at the fixed point is given by

$$\begin{pmatrix} \dot{x} \\ \dot{y} \end{pmatrix} = J^{\mathrm{II}} \begin{pmatrix} x \\ y \end{pmatrix} + \begin{pmatrix} 0 \\ h(x,y) \end{pmatrix}, \tag{A1}$$

where J^{II} is the Jacobian for model II given by Eq. (22), and

$$h(x,y) = Axy + By^2 + Cxy^2 + Dy^3. \tag{A2}$$

Here the coefficients are given by

$$A = 2\,\theta_{\mathrm{ss}}\alpha,$$

$$B = 2\,\theta_{\mathrm{ss}}\alpha - \frac{1}{\theta_{\mathrm{ss}}\tau},$$

$$C = \alpha,$$

$$D = \alpha. \tag{A3}$$

We perform a linear transformation so that Eq. (A1) is cast in the normal form [30], where the matrix elements of the Jacobian operator are the real and imaginary parts of the complex eigenvalues $\lambda = \gamma \pm i\Omega$. That is, we define a coordinate transformation in terms of the linear operator S such that

$$S^{-1} J^{\mathrm{II}} S = \begin{pmatrix} \gamma & \Omega \\ -\Omega & \gamma \end{pmatrix}. \tag{A4}$$

Following standard techniques from linear algebra S and S^{-1} are obtained from the real and imaginary parts of the eigenvectors of J^{II}:

$$S = (v_r v_i) = \begin{pmatrix} 1 & 0 \\ (-1-\gamma) & -\Omega \end{pmatrix} \tag{A5}$$

and

$$S^{-1} = \frac{-1}{\Omega} \begin{pmatrix} -\Omega & 0 \\ (1+\gamma) & 1 \end{pmatrix}. \tag{A6}$$

Next we implement the linear change of variables

$$\begin{pmatrix} w \\ z \end{pmatrix} = S^{-1} \begin{pmatrix} x \\ y \end{pmatrix} \tag{A7}$$

in Eq. (A1), in order to express this system in the normal form

$$\begin{pmatrix} \dot{w} \\ \dot{z} \end{pmatrix} = \begin{pmatrix} \gamma & \Omega \\ -\Omega & \gamma \end{pmatrix} \begin{pmatrix} w \\ z \end{pmatrix} + \begin{pmatrix} f(w,z) \\ g(w,z) \end{pmatrix} \tag{A8}$$

with $f(w,z)=0$, $g(w,z)=-h(w,-w-\Omega z)/\Omega$, and $h(x,y)$ as in Eq. (A2).

The condition $\gamma=0$ corresponds to the Hopf bifurcation point. The stability coefficient a_1 determines whether the bifurcation is subcritical or supercritical, and is calculated using the nonlinear terms. The advantage in changing variables as we have done above, is that it allows us to apply the standard formula (see Ref. [28]), which in our case reduces to

$$a_1 = \frac{1}{16}[g_{wwz}+g_{zzz}] - \frac{1}{16\Omega}[g_{wz}(g_{ww}+g_{zz})]. \tag{A9}$$

Here Ω and the partials of $g(w,z)$ are evaluated at the Hopf bifurcation point. They are

$$\Omega = \frac{1}{\sqrt{\tau}},$$

$$g_{ww} = 2(A-B)/\Omega = \frac{2}{\Omega \tau \theta_{ss}^{II}},$$

$$g_{wz} = A - 2B = 2\left(\frac{1}{\theta_{ss}^{II}\tau} - \theta_{ss}^{II}\alpha \right),$$

$$g_{zz} = -2B\Omega = -2\Omega\left(2\theta_{ss}^{II}\alpha - \frac{1}{\theta_{ss}^{II}\tau} \right),$$

$$g_{wwz} = 2(3D-2C) = 2D = 2\alpha,$$

$$g_{zzz} = 6D\Omega^2 = \frac{6\alpha}{\tau}. \tag{A10}$$

Finally we obtain

$$a_1 = \frac{\alpha}{8}\left(\frac{3}{\tau} - 1 \right). \tag{A11}$$

From Eq. (A11) in these (dimensionless) units for model II $a_1>0$ for $\tau<3$, $a_1=0$ for $\tau=3$, and $a_1<0$ for $\tau>3$. For model I the corresponding calculation yields $a_1=0$ regardless of the other parameter values, which alone is inconclusive and requires a higher order nonlinear analysis [31].

When the parameters are close to those associated with the bifurcation point and for initial conditions which are in the neighborhood of the fixed point a quasilinear transformation from the (w,z) coordinate system to one described by polar coordinates (r,ϕ) yields the following leading order equations for the amplitude and phase of the oscillatory solution:

$$\dot{r} = r(\gamma + a_1 r^2) + O(r^5), \tag{A12}$$

$$\dot{\phi} = \Omega + O(r^2). \tag{A13}$$

The Hopf theorem asserts that the phase flow of these equations is topologically equivalent to that of the full nonlinear system near the fixed point [28]. Beyond the bifurcation point $\gamma>0 (V<V_H)$, so that if $a_1<0$ there is a stable limit cycle with $r=\sqrt{-\gamma/a_1}$, and the transition is predicted to be continuous (a supercritical bifurcation), while if $a_1>0$ the transition is discontinuous (a subcritical bifurcation) with an unstable limit cycle at $r=\sqrt{-\gamma/a_1}$.

For model II we obtain $\gamma=-\sqrt{(\alpha/\tau)(\tau+1)^3}\Delta V$, where $\Delta V=(V-V_H^{II})$. Substituting in this expression, Eq. (A11) and reintroducing the dimension from Eq. (6) we obtain the following dependence of the expected radius of the limit cycle on the stiffness k:

$$r = \left(\frac{8\beta[k/(\sigma^3\alpha)]^{1/2}(k\tau/\beta+1)^{3/2}}{[3\beta/(k\tau)-1]} \Delta V \right)^{1/2}. \tag{A14}$$

Because the amplitude of the stick slip oscillations are of (essentially) fixed finite value, the dependence of the radius of the unstable limit cycle on ΔV determines the width of the hysteresis loop. When $k \gg 1$ but still less than $3\beta/\tau$, r grows rapidly as ΔV increases. On the other hand, as $k \to 0$, $r \propto \sqrt{k\Delta V}$. This as $k \to k_{max}$ which marks the end of the stick-slip regime, the hysteresis loop is expected to become increasingly narrow, and as $k \to 0$ we expect the hysteresis gap to widen, consistent with our numerical results shown in Fig. 6.

While our experimentally estimated parameter values have led us to focus primarily on a regime in which the transition remains subcritical throughout the dynamical phase diagram, other parameter values can yield a phase boundary in which there is a crossover from a subcritical (at small k) to a supercritical (at large k) transition at $k=3\beta/\tau$. The predicted radius of the orbit Eq. (A14) diverges at the value of k associated with the crossover, which suggests the transition will be extremely sharp, and thus very difficult to distinguish numerically from the discontinuous case.

[1] A review of recent progress on both fundamental and applied problems involving friction is given in *Fundamentals of Friction: Macroscopic and Microscopic Processes*, edited by I. L. Singer and H. M. Pollock, Vol. 220 of *Nato Advanced Study Institute, Series E: Applied Science* (Kluwer, Dordrecht, 1992).

[2] An introduction to friction and control, as well as a summary of several rate and state constitutive relations (referred to as ''dynamic friction models'') which have been introduced recently in the context of engineering systems is discussed in H. Olsson, Ph.D. thesis, Department of Automatic Control, Lund Institute of Technology, Lund, Sweden, 1996.

[3] See, e.g., *Handbook of Micro/Nano Tribology*, edited by B.

Bhushan, *CRC Series on Mechanics and Materials Science* (CRC, New York, 1995).
[4] J. N. Israelachvili, P. M. McGuiggan, and A. M. Homola, Science **240**, 189 (1988).
[5] M. L. Gee, P. M. McGuiggan, and J. N. Israelachvili, J. Chem. Phys. **93**, 1895 (1990).
[6] H. Yoshisawa and J. N. Israelachvili, J. Phys. Chem. **97**, 11 300 (1993).
[7] S. Granick, Science **253**, 1374 (1991).
[8] G. Reiter, A. L. Demirel, and S. Granick, Science **263**, 1741 (1994); G. Reiter, A. L. Demirel, J. Peansky, L. L. Cai, and S. Granick, J. Chem. Phys. **101**, 2606 (1994).
[9] P. A. Thompson, G. S. Grest, and M. O. Robbins, Phys. Rev. Lett. **68**, 3448 (1992).
[10] A. D. Berman, W. A. Ducker, and J. N. Israelachvili, Langmuir **12**, 4559 (1996).
[11] A. Ruina, J. Geophys. Res. **88**, 10 359 (1983).
[12] J. H. Dieterich, Pure Appl. Geophys. **116**, 790 (1978); J. Geophys. Res. **84**, 2161 (1979); J. H. Dieterich and B. D. Kilgore, PAGEOPH **143**, 283 (1994).
[13] J. R. Rice and A. L. Ruina, J. Appl. Mech. **105**, 343 (1983).
[14] L. A. Reinen, J. D. Weeks, and T. E. Tullis, Geophys. Res. Lett. **18**, 1921 (1991).
[15] J. R. Rice and S. T. Tse, J. Geophys. Res. **91**, 521 (1986).
[16] J.-C. Gu, J. R. Rice, A. L. Ruina, and S. T. Tse, J. Mech. Phys. Solids **32**, 167 (1984).
[17] C. Gao, D. Kuhlmann-Wilsdorf, and D. Makel, Wear **173**, 1 (1994).
[18] Y. Gu and T.-F. Wong, Nonlin. Dyn. Pred. Geophys. Phen. **18**, 15 (1994).
[19] J. M. Carlson and A. A. Batista, Phys. Rev. E **53**, 4153 (1996).
[20] J. M. Carlson and A. Berman (unpublished).
[21] A linear stability analysis of model I was also presented in B. Persson, Chem. Phys. Lett. **254**, 114 (1996).
[22] P. A. Thompson and M. O. Robbins, Phys. Rev. A **41**, 6830 (1990).
[23] N. M. Beeler, T. E. Tullis, and J. D. Weeks, Geophys. Res. Lett. **21**, 1987 (1994).
[24] T. Baumberger, F. Heslot, and B. Perrin, Nature (London) **367**, 544 (1994).
[25] T. Baumberger, C. Caroli, B. Perrin, and O. Rosnin, Phys. Rev. E **51**, 4005 (1995).
[26] Experiments on molecularly thin melted films at high constant shear rates reveal shear-thinning, which modifies the simple linear dependence of the friction on the shear rate which is characteristic of Newtonian fluids. Typically the viscosity scales as $V^{-2/3}$, so that overall the friction increases as $V^{1/3}$ at high shear rates. We ignore that feature and assume a constant viscosity.
[27] The viscosity of extremely confined fluids is approximately six orders of magnitude higher than that of a fluid in the bulk [C. Drummond (private communication)]. For a lubricant such as OMCTS the viscosity when confined is $\eta \approx 6 \times 10^5$ Pa s. Our estimate of $\beta = \eta A/h$ is obtained from this assuming a contact of diameter of approximately 10 μm and a distance between the mica sheets of around 1 nm.
[28] J. Guckenheimer and P. Holmes, *Nonlinear Oscillations, Dynamical Systems, and Bifurcations of Vector Fields* (Springer-Verlag, New York, 1983), Chap. 3.
[29] W. Press, S. Teukolsky, W. Vetterling, and B. Flannery, *Numerical Recipes in C*, 2nd ed. (Cambridge University Press, New York, 1995).
[30] P. Glendinning, *Stability, Instability and Chaos* (Cambridge University Press, New York, 1994), Sec. 3.2.
[31] While a higher order nonlinear analysis of Eqs. (8) is certainly possible, the calculation involves an enormous number of terms.